Anal. Chem. **2000,** *72,* 3030−3037

Turn Geometry for Minimizing Band Broadening in Microfabricated Capillary Electrophoresis Channels

Brian M. Paegel, Lester D. Hutt, Peter C. Simpson,† and Richard A. Mathies*

Department of Chemistry, University of California, Berkeley, California 94720

Turns in microfabricated capillary electrophoresis channels generally result in degraded separation quality. To circumvent this limitation, channels were constructed with different types of turns to determine the design that minimizes turn-induced band broadening. In particular, tapered turns were created by narrowing the separation channel width before the start of a turn and widening the channel after the turn is complete. The radius of curvature of the turn, the length over which the channel is tapered, and the degree of tapering were explored. The column efficiencies were determined by examining the resolution of the 271/281 base pair doublet in the separation of a ϕX174 *Hae*III DNA sizing ladder. Tapered turns with the smallest radius of curvature (250 μm), the shortest tapering length between the separation and turn widths (55 μm), and the largest tapering ratio (4:1 separation channel width to turn channel width) produced the highest resolution separations. These results are discussed by comparison to theoretical predictions of the effect of tapers and turns on analyte band dispersion in capillary electrophoresis.

The microfabrication of capillary electrophoresis (CE) devices on planar glass substrates enhances the performance of electrophoretic analyses[1−3] and is leading to the development of new classes of integrated microfluidic devices.[4] For example, ultrafast DNA fragment sizing,[5,6] short tandem repeat (STR) analysis,[7] and DNA sequencing[8−10] have been demonstrated. More complex multichannel devices have been developed by employing wafer-scale integration to perform high-throughput genotyping of 12, 48, and 96 samples in parallel.[11−13] The integration of PCR reactors and electrochemical detection has also been reported.[14,15] This increased device complexity has often necessitated the incorporation of turns in channels to facilitate wafer-scale integration. When an electrophoresis channel is used for transport and/or low-resolution separations, these turns have little impact on the quality of the separation. However, when turns are used to extend the column length to perform high-resolution separations, the separation quality can be significantly compromised.[16]

The introduction of turns and the impact of turns on device performance was considered in the early literature on microchip electrophoresis.[17] Seiler and co-workers[17] fabricated devices with right angle turns, but noticed no degradation in the quality of capillary zone electrophoresis (CZE) separations. Later work[16] reexamined a serpentine channel geometry and presented videomicroscopy evidence that turns noticeably degrade the band shape and overall separation efficiency. A detailed account of capillary coiling and its effect on band broadening[18] revealed that conventional CE exhibits the same geometry-related band broadening observed in microchips. Theoretical analyses of the resolution of chip-based separations have been presented and band broadening due to turns has been linked directly to the angle of the turn and to the width of the separation channel.[16] The reduced efficiency was found to be due to path length differences between molecules traveling along the outer radius and the inner radius of the turn.

* Corresponding author: (fax) (510) 642-3599; (e-mail) rich@zinc.cchem.berkeley.edu.

† Present address: Kiva Genetics Inc., 2375 Garcia Ave., Mountain View, CA 94043.

(1) Manz, A.; Harrison, D. J.; Verpoorte, E. M. J.; Fettinger, J. C.; Paulus, A.; Ludi, H.; Widmer, H. M. *J. Chromatogr.* **1992**, *593*, 253−258.
(2) Harrison, D. J.; Manz, A.; Fan, Z. H.; Ludi, H.; Widmer, H. M. *Anal. Chem.* **1992**, *64*, 1926−1932.
(3) Harrison, D. J.; Fan, Z. H.; Seiler, K.; Manz, A.; Widmer, H. M. *Anal. Chim. Acta* **1993**, *283*, 361−366.
(4) *Micro Total Analysis Systems 2000*; Kluwer Academic Publishers: Dordrecht, The Netherlands, 2000.
(5) Woolley, A. T.; Mathies, R. A. *Proc. Natl. Acad. Sci. U.S.A.* **1994**, *91*, 11348−11352.
(6) Effenhauser, C. S.; Paulus, A.; Manz, A.; Widmer, H. M. *Anal. Chem.* **1994**, *66*, 2949−2953.
(7) Schmalzing, D.; Koutny, L.; Adourian, A.; Belgrader, P.; Matsudaira, P.; Ehrlich, D. *Proc. Natl. Acad. Sci. U.S.A.* **1997**, *94*, 10273−10278.
(8) Woolley, A. T.; Mathies, R. A. *Anal. Chem.* **1995**, *67*, 3676−3680.
(9) Liu, S.; Shi, Y.; Ja, W. W.; Mathies, R. A. *Anal. Chem.* **1999**, *71*, 566−573.
(10) Schmalzing, D.; Adourian, A.; Koutny, L.; Ziagura, L.; Matsudaira, P.; Ehrlich, D. *Anal. Chem.* **1998**, *70*, 2303−2310.
(11) Woolley, A. T.; Sensabaugh, G. F.; Mathies, R. A. *Anal. Chem.* **1997**, *69*, 2181−2186.
(12) Simpson, P. C.; Roach, D.; Woolley, A. T.; Thorsen, T.; Johnston, R.; Sensabaugh, G. F.; Mathies, R. A. *Proc. Natl. Acad. Sci. U.S.A.* **1998**, *95*, 2256−2261.
(13) Shi, Y.; Simpson, P. C.; Scherer, J. R.; Wexler, D.; Skibola, C.; Smith, M. T.; Mathies, R. A. *Anal. Chem.* **1999**, *71*, 5354−5361.
(14) Woolley, A. T.; Hadley, D.; Landre, P.; deMello, A. J.; Mathies, R. A.; Northrup, M. A. *Anal. Chem.* **1996**, *68*, 4081−4086.
(15) Woolley, A. T.; Lao, K.; Glazer, A. N.; Mathies, R. A. *Anal. Chem.* **1998**, *70*, 684−688.
(16) Jacobson, S. C.; Hergenroder, R.; Koutny, L. B.; Warmack, R. J.; Ramsey, J. M. *Anal. Chem.* **1994**, *66*, 1107−1113.
(17) Seiler, K.; Harrison, D. J.; Manz, A. *Anal. Chem.* **1993**, *65*, 1481−1488.
(18) Kasicka, V.; Prusik, Z.; Gas, B.; Stedry, M. *Electrophoresis* **1995**, *16*, 2034−2038.

10.1021/ac000054r CCC: $19.00
Published on Web 06/01/2000

This problem is exacerbated in situations involving electrokinetic transport where molecular velocity is determined by electric field strength. Because the path length is greater along the outer radius, the electric field along the outer track is smaller and molecules will also have a lower electrophoretic velocity.

The research presented here considers the parameters that cause turn-induced band broadening and investigates methods by which turns may be geometrically modified to reduce that variance. Specifically, we have fabricated tapered turns where the width of the channel in the turn is reduced with the goal of reducing the path length difference between the inner and outer radii. The effects of the radius of curvature of the turn, the length of the tapered region, and the width of the channel in the turn are explored. These trends are analyzed in the context of previously discussed models describing the effect of tapers and turns on electrophoretic band migration.

EXPERIMENTAL SECTION

Microfabrication. Chip fabrication was performed according to previously published procedures[12,19] at the U.C. Berkeley Microfabrication Laboratory. Briefly, Borofloat wafers (10 cm diameter × 1.1 mm; Precision Glass and Optics, Santa Ana, CA) were coated with a 1500-Å amorphous silicon sacrificial mask in a low-pressure chemical vapor deposition (LPCVD) furnace. The wafers were baked at 120 °C and then primed for 5 min with hexamethyldisilazane. The primed wafers were spin-coated with photoresist (1818, Shipley, Marlborough, MA) at 5000 rpm for 30 s and soft-baked for 5 min on a 90 °C hot plate. The channel pattern was transferred to the coated substrate using a contact printer (Quintel Corp., San Jose, CA) and developed using Microposit developer (1:1 with deionized water, Shipley). The masked channel widths were 110 μm for separation channels and 30 μm for injection cross channels. The amorphous silicon was removed in the developed areas via plasma etching, and the exposed glass was wet-etched for 120 s in 49% HF producing trapezoidal channels 14 μm deep with final separation and cross-injector channel widths of 138 and 58 μm, respectively. Once the remaining photoresist and amorphous silicon were stripped, 1.2-mm-diameter access holes were drilled for the sample, cathode, and waste reservoirs, while the central anode reservoir was 2 mm in diameter. The drilled plate was thermally bonded to a blank cover plate. The channels were coated according to the Hjerten protocol[20] to suppress electroosmotic flow and to prevent adsorption of DNA.

Sample Preparation and Separation Conditions. A *Hae*III digest of ϕX174 bacteriophage DNA (New England Biolabs, Beverly, MA) was diluted to 30 ng/μL in pH 8.2 1× Tris-acetate/EDTA (TAE) buffer (40 mM Tris, 40 mM acetate, 1 mM EDTA). For the sieving matrix, 438 000 molecular weight hydroxyethylcellulose (HEC) was dissolved in 1× TAE to 0.75% w/v. Thiazole orange (TO), an intercalating dye used for fluorescent labeling of DNA fragments,[21] was diluted to 1 μM working concentration in the sieving matrix, and the mixture was degassed under vacuum with stirring for 10 min. The degassed mixture was centrifuged to remove particulate matter and bubbles prior to injection.

The degassed HEC solution was applied to the central anode with a syringe and forced through the array of channels. The DNA sample (2.2 μL) was placed in each sample reservoir, 2.2 μL of 1× TAE run buffer was placed in each waste and cathode reservoir, and 6 μL of run buffer was placed in the central anode to make electrical contact with the electrodes. A network of electrodes was fabricated to facilitate the application of the voltages delivered by four power supplies to the eight separation systems simultaneously. To perform the pinched injection, sample was electrophoresed at 700 V/cm for 30 s from the sample reservoir to the waste reservoir (100 V applied to the sample reservoir and 400 V applied to the waste reservoir) while holding the anode and cathode at 150 V to confine the sample to the injection intersection. The field was then switched to electrophorese the sample down the separation column at 300 V/cm (100 V applied to the cathode and 1500 V applied to the anode). A back-biasing electric field of 33 V/cm was applied between the injection cross point and both the sample and waste reservoirs to avoid sample bleed and to optimize the injection plug shape.

Detection System and Data Acquisition. The radially arrayed channels were interrogated using a radial scanning confocal fluorescence detection system, which has been described in detail elsewhere.[13] Excitation (30 mW) from an argon ion laser (Spectra-Physics 2017, Mountain View, CA) operating at 488 nm was focused on the channel through a 20 × 0.5 NA achromatic objective (Rolyn Optics, Covina, CA) to excite the DNA−TO complex. The laser was scanned at 4 Hz in a 1-cm-radius circle by a computer-controlled stepper motor. Fluorescence gathered by the objective was spectrally filtered using a 30-nm band-pass filter at 520 nm (Omega Optical, Brattleboro, VT) and spatially filtered using a 150-μm pinhole. Signal from the PMT was electronically filtered using an analog 5.76-kHz low-pass filter (SR640, Stanford Research Systems, Sunnyvale, CA). Filtered data were digitized using a 3400a data acquisition processor (Microstar Laboratories, Bellevue, WA) that sampled the 6.28-cm scan circumference at 2840 points/revolution with 12-bit resolution. Data were stored as an image file in tagged image file format (TIFF). At 2840 pixels/revolution, each 138-μm-wide channel was defined by 10 pixels ~14 μm on a side.

The TIFF files were processed using IPLab image processing software (Signal Analytics, Vienna, VA) to generate electropherograms for analysis. Channels were cropped from the image, and rows of pixels corresponding to the same time were averaged to produce each electropherogram. An average of seven data points in the time coordinate defined each DNA peak in each electropherogram. The final electropherograms were loaded into Igor Pro spectral analysis software (Wavemetrics Inc., Lake Oswego, OR), and Gaussian peak profiles were fit to the 271- and 281-base pair (bp) peaks to determine the resolution.

THEORY

In these experiments, tapered turns are constructed by narrowing the channel before the turn, completing the 180° turn with a channel of reduced width, and widening the channel after the turn. The key variables of this geometry are defined in Figure 1. The width in the separation portion and in the turn portion are

(19) Simpson, P. C.; Woolley, A. T.; Mathies, R. A. *Biomed. Microdevices* **1998**, *1*, 7−26.
(20) Hjerten, S. *J. Chromatogr.* **1985**, *347*, 191−198.
(21) Zhu, H.; Clark, S. M.; Benson, S. C.; Rye, H. S.; Glazer, A. N.; Mathies, R. A. *Anal. Chem.* **1994**, *66*, 1941−1948.

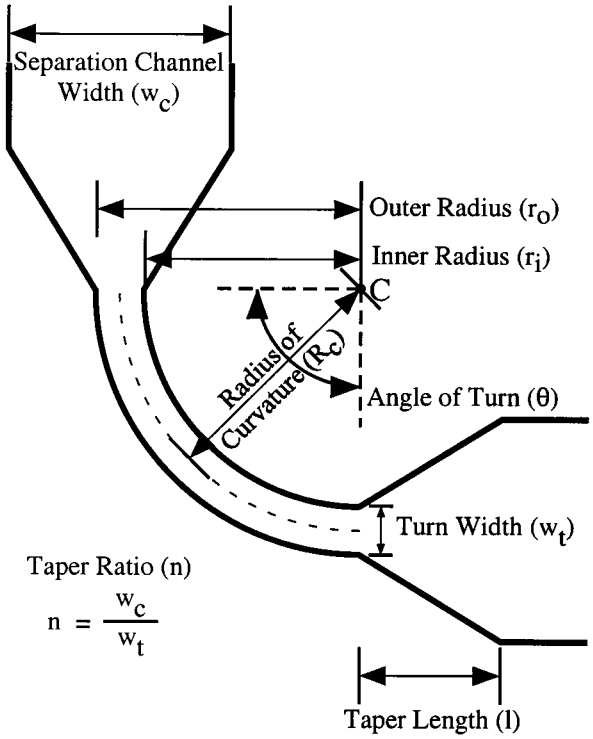

Figure 1. Defining parameters of a tapered turn in a microfabricated channel. The width of the channel in the turn is denoted w_t and the width in the separation channel is defined as w_c. The turn subtends an arc of θ rad with a radius of curvature R_c. The width, w_t, can also be defined in terms of the inner and outer radii of the channel, r_i and r_o,respectively.

denoted w_c and w_t, respectively. The ratio of these widths, w_c/w_t, is defined as the taper ratio, n. The turn may also be described by the outer and inner radii of the channel denoted r_o and r_i, respectively. The radius of curvature of the turn (defined as the average of r_o and r_i) is R_c, and the angle of the turn is denoted θ. The length of the channel over which the taper is achieved is defined in terms of the tapering length, l.

A theory on the effect of turns on electrophoretic separations in microfabricated channels has been published elsewhere.[22] The following treatment is focused on the equations that have a direct impact on this work. The path lengths along the inner and outer radii of the turn, L_i and L_o, are defined by

$$L_i = \theta r_i \qquad \text{and} \qquad L_o = \theta r_o \tag{1}$$

Analytes with an electrophoretic mobility, μ, have a velocity, v, proportional to the local electric field strength, E, which is different along the inner and outer paths:

$$v_i = \mu E_i \qquad \text{and} \qquad v_o = \mu E_o \tag{2}$$

The local electric field strength (V/cm) is defined by the voltage applied across the turn, U, and the length over which the field is applied. The time required to travel a given length, t, is given by the length over the velocity. Combining these facts with eqs 1 and 2 and assuming diffusion effects are negligible gives

$$t_i = (\theta r_i)^2/\mu U \qquad \text{and} \qquad t_o = (\theta r_o)^2/\mu U \tag{3}$$

The difference in transit time along the inner and outer radii is then

$$\Delta t = \theta^2(r_o^2 - r_i^2)/\mu U = 2\theta^2 R_c w_t/\mu U \tag{4}$$

The expression can be simplified by recognizing that the separation electric field, E, is identical to the electric field along the arc subtended by the radius of curvature. Using this relation and converting eq 4 to a time-based standard deviation, we have

$$\sigma_{turn} = \theta w_t/\mu E \tag{5}$$

Equation 5 indicates that turns with the smallest channel widths and turn angles will exhibit lower turn-induced band broadening.

The primary effect of a taper in a microfabricated channel can be understood using a simplified two-dimensional model. Reasonably assuming that the channel depth is constant, a band can be described by its width and length, or area. The width of a band is constrained by the physical width of the channel. The band has a width, w_c, while traversing straight portions of the channel, and it has a width, w_t, while occupying a turn region. Likewise, the length of the band can be denoted l_c and l_t in the channel and turn, respectively. Using these parameters, the area of the band confined in the separation channel is defined as

$$A = w_c l_c \tag{6}$$

The band is then moved into the turn portion of the channel that has been constructed with a taper ratio of n. Due to the constricted channel width, the local electric field is enhanced by a factor of n. Continuity dictates that the length of the band will increase in the turn:

$$A = w_c l_c = w_t l_t = \left(\frac{w_c}{n}\right)(n l_c) \tag{7}$$

While the band is in the turn, it will be broadened by diffusion and by the geometry of the turn. Symbolically, this is represented by added length δl. The new area of the band, prior to exiting the turn, is thus given by

$$A = \left(\frac{w_c}{n}\right)(n l_c + \delta l) \tag{8}$$

When the band exits the turn and proceeds through the exit-side taper, the bandwidth is returned to w_c and the band length is commensurately decreased by a factor of $1/n$ to satisfy continuity. This can be described by

$$A = (w_c)\left(l_c + \frac{\partial l}{n}\right) \tag{9}$$

(22) Culbertson, C. T.; Jacobson, S. C.; Ramsey, J. M. *Anal. Chem.* **1998**, *70*, 3781−3789.

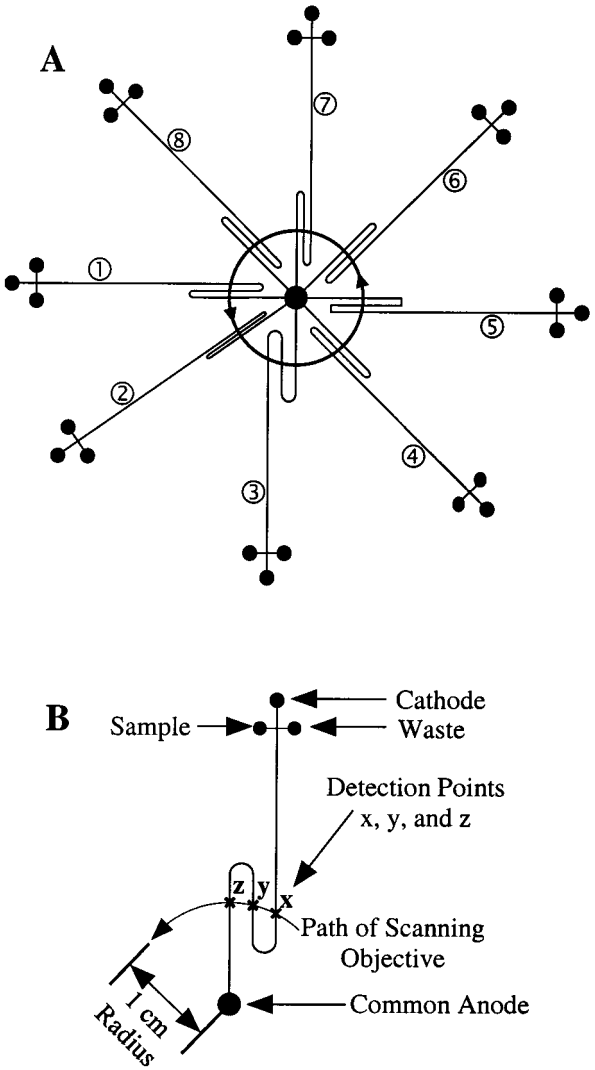

Figure 2. (A) Layout of the microplate. The 1-cm-radius path of the scanning objective is indicated by the arrow. The parameters of the turns in each channel are summarized in Table 1. (B) Magnified view of a single channel. The sample, waste, and cathode reservoirs were fabricated 3 mm from the injection cross. The 14-μm-deep separation channels were 138 μm wide and the injection cross-channels were 44 μm wide. The scanning objective monitored the separation at points *x*, *y*, and *z* placed 2.75, 3.82, and 4.93 cm, respectively from the injection cross.

The δl term will also be reduced by a factor determined exclusively by the taper ratio. This process of returning a band to its original width shall be referred to as "band compression" in the ensuing discussion.

RESULTS AND DISCUSSION

The design of the microplate is shown in Figure 2. Eight geometrically different folded channels were arrayed around a central anode reservoir. The scanning objective followed a 1-cm-radius circular path centered on the anode. Each channel was sampled at three detection points (*x*, *y*, and *z*) that were placed 2.75, 3.82, and 4.93 cm, respectively, from the injection cross. The detection points were defined by aligning the central anode reservoir with the axis of rotation of the scanning objective. Each channel was designed with two complementary and geometrically identical 180°-turn structures. One parameter of the turn design was varied for each channel while the other parameters were held constant. The first four columns of Table 1 summarize the geometric variations that were made. The channels will be referred to by the numerical labeling in Table 1 and in Figure 2A.

The radial arrangement of channels and scanning detection avoided several significant sources of experimental variance that were observed in single-channel experiments. Single-channel detection schemes require multiple injections on the same column, which entails refilling the column with matrix between injections and reproducibly positioning the chip to define the same detection point. Variations in the injected plug properties and especially variations in the separation matrix properties were found to mask the turn-induced effects being probed here. The presented microplate layout uniquely allowed us to monitor every separation at three different points, thereby producing a self-consistent data set for each experiment.

The channel designs yield four different experimental comparisons. Figure 3 presents electropherograms generated from the images collected at each detection point for channels 4, 5, and 7. In Figure 3A, the electropherograms show that the separation is of high quality before the turn at point *x*, but after the first square turn, the separation is degraded as observed at point *y*, and the separation does not improve after additional electrophoresis to point *z*. After the first square turn, the image shows that the band is tilted and distorted. The second turn does not correct the effects of the first turn and the bands at point *z* are further distorted.

The U-shaped turns shown in Figure 3B produce a good electrophoretic peak shape at point *x* and resolution of fragments of similar sizes. At point *y*, the first turn has skewed the bands in the channel and this produces broad peaks in the electropherogram. At point *z*, the analytes have traversed the second turn, and the skew has been removed. However, the bands are diffuse as evidenced by the lower signal intensity in the electropherogram for point *z* compared to point *x*, and the observation that the resolution at point *z* is only slightly better than that at point *x*.

The tapered turn design shown in Figure 3C also produces good band shape and resolution at point *x*. The separation exhibits slight band skewing after the first turn (point *y*). The image shows that the slight band tilting has been corrected and the resolution has improved after the second turn. The normalized resolution of the 271- and 281-bp peaks at point *z* was 0.8, 1.1, and 1.4 for the square, U-shaped, and tapered turns, respectively.

This initial comparison provides qualitative evidence that separations in channels containing turns are heavily influenced by the geometric parameters of the turn. Square and U-shaped turns produce separations with tilted and distorted bands, and as a consequence, the analyte signals are less intense and exhibit distorted peak shapes with poorer resolution. A portion of the reduced resolution in the electropherograms is due to the data acquisition and reduction method. The electropherograms are produced by signal averaging a row of pixels orthogonal to the long axis of the separation channel. When this process is carried out for a tilted band, broader peaks are observed. When the tilted band encounters the complementary turn, the tilt is reversed and the resolution improves. However, while traversing the channel

Table 1. Channel Turn Parameters and Results

channel no.	radius of curvature R_c (μm)	taper length l (μm)	taper ratio n	best-fit slope[a] (cm^{-1})	R^2	std dev of slope	data point uncertainty[b] (%)	no. of measmts
1	500	200	2	0.09	0.9272	0.02	10 5 7	10
2	250	200	4	0.208	0.9972	0.008	6 3 3	10
3	1000	200	4	0.134	0.9934	0.007	4 5 4	9
4	500	0	1	0.04	0.0274[c]	0.2[c]	17 60 14	6
5[d]	500	0	1	−0.09	0.5486[c]	0.06[c]	13 4 5	6
6	500	55	4	0.196	0.9992	0.004	11 9 6	7
7	500	200	4	0.185	0.9967	0.007	11 8 7	10
8	500	800	4	0.164	0.9973	0.006	12 10 8	7

[a] For a given set of three data points (x, y, z) from a single separation, the best-fit slope was computed for normalized resolution vs effective column length. These slopes were averaged to yield the slope reported for an individual channel. Absolute resolutions were observed to have a relative error of ∼10%; the averaged slopes had a relative error of ∼2%. [b] Uncertainties are listed for detection at 2.75, 3.82, and 4.93 cm, respectively. [c] Low R^2 values are due to the data acquisition method as discussed in the text. [d] Channel 5 is the square turn channel.

in the tilted orientation, transverse diffusion widens the band; this diffusion as well as the turn-induced distortion are not counteracted by passage through a complementary turn.

The remaining three experimental comparisons explore the performance of tapered turns having different turn parameters. In the second comparison, channels 1, 4, and 7 vary n while fixing R_c. While the taper length, l, in the second comparison changed as n is increased, the taper angle was kept constant. In the third comparison, channels 2, 3, and 7 vary R_c while keeping l and n constant. In the final experiment, channels 6, 7, and 8 vary l while keeping R_c and n constant. For each channel comparison, the resolution was calculated for the 271- and 281-bp peaks and plotted versus effective column length. Linear least-squares analysis was used to determine the best-fit line for these plots (Figure 4). This operation was carried out for each separation. The least-squares slopes for each set of three data points on a given channel were then averaged. The averaged least-squares slopes, correlation coefficients, number of experiments averaged, standard deviation of the slope data set, and relative errors in each data point are summarized in Table 1. Qualitatively, the data in Figure 4 reveal several trends that are important in the selection of optimal turn designs.

Turn Geometry. Tapered turn designs are superior to comparable U-shaped turns and square-corner turns (Figure 4A). The resolution per unit length for the tapered turn is 4 times greater than that of U-shaped turn. While both U-shaped and tapered designs exhibit increases in resolution at longer column lengths, the square turns are so detrimental to the separation quality that the resolution decreases as the column length is increased.

Taper Ratio Effect. Turns with an increased taper ratio produce improved separations (Figure 4B). According to eq 5, the band variance is described by

$$\sigma_{\text{turn}}{}^2 = (\theta w_t/\mu E)^2 \tag{10}$$

Therefore, σ_{turn} is linearly proportional to w_t. The resolution function is inversely proportional to the standard deviation of the peaks assuming they are Gaussian giving

$$R = \frac{t_2 - t_1}{(1/2)(w_1 + w_2)} = \frac{\Delta t}{2(\sigma_1 + \sigma_2)} \tag{11}$$

where t_1 and t_2 are the retention times of two peaks and σ_1 and σ_2 are the time-based standard deviations of the two peaks. Using the previous definition of n, eq 10 can be substituted into eq 11 giving

$$R = \Delta t n \mu E / 4\theta w_c \tag{12}$$

where we have assumed that the electrophoretic mobilities of the two analytes of interest are approximately equal (as is the case for the 271/281-bp doublet) and that the turn-induced variance is the dominant contributor to the overall expression for band variance and is identical for both peaks. As predicted, the slopes of the best-fit lines of resolution as a function of column length in Figure 4B increased. Figure 5 presents a plot of the resolution per unit column length versus taper ratio. The column efficiency is linearly proportional to the taper ratio.

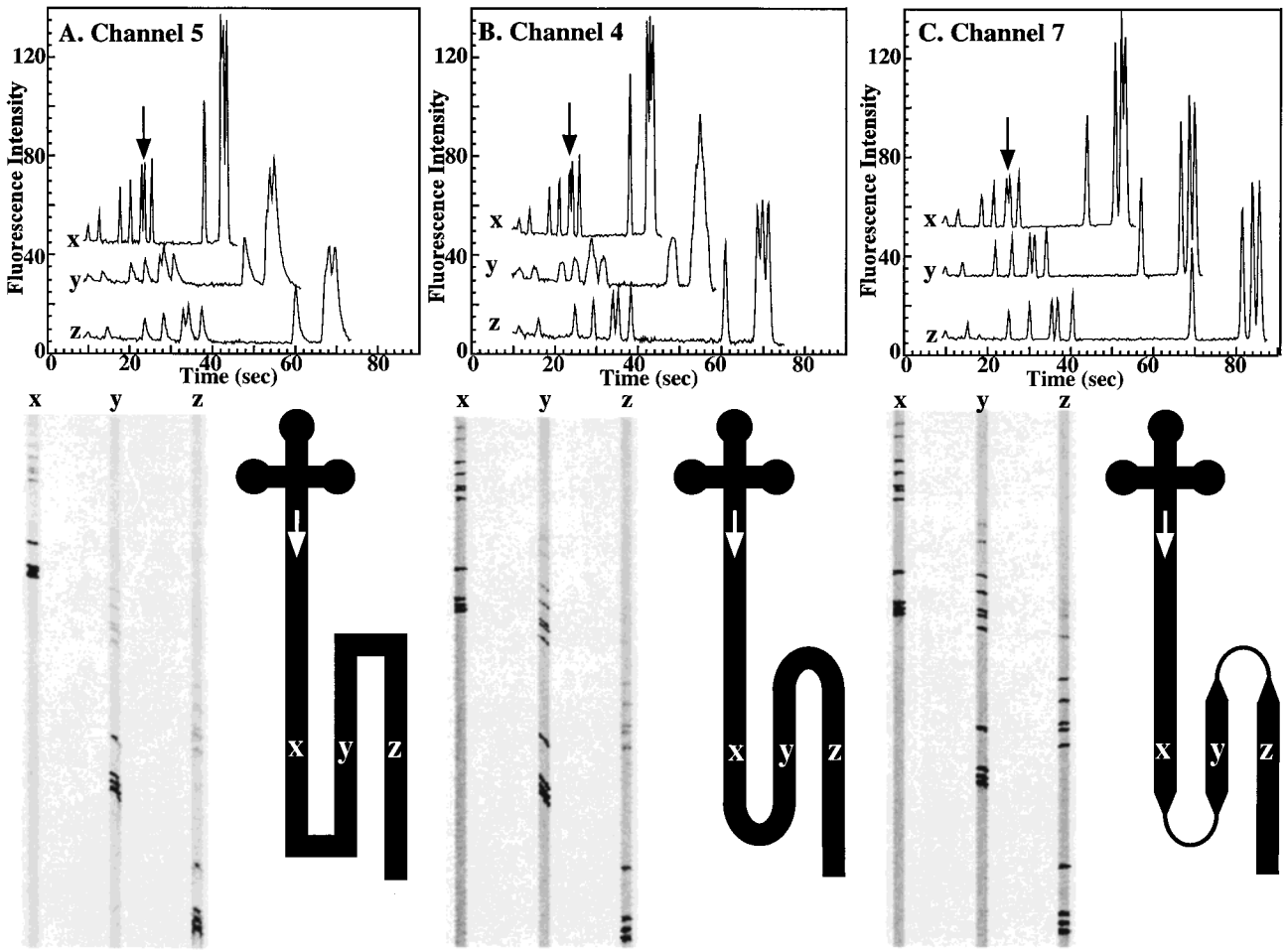

Figure 3. Electropherograms measured at detection points *x*, *y*, and *z* for channels 5, 4, and 7. An image of the separation and the channel design are given below each set of electropherograms. (A) The square turn, channel 5. (B) The U-shaped turn, channel 4. (C) A tapered turn with $R_c = 500\ \mu$m, $l = 200\ \mu$m, and $n = 4{:}1$, channel 7. The fragments of the ϕX174 *Hae*III digest DNA ladder are of lengths 72, 118, 194, 234, 271, 281, 310, 603, 872, 1078, and 1353 base pairs. The 271- and 218-bp peaks are indicated by the arrow. The channel designs are not drawn to scale.

Radius of Curvature. The resolution per unit channel length improves as R_c is reduced (Figure 4C). When R_c is reduced from 1000 to 500 μm, the resolution per length of column increases from 0.134 to 0.185 cm^{-1}. Further reduction of R_c to 250 μm resulted in an increase of the resolution to 0.208 cm^{-1}. This trend was not expected from the basic theory on the effects of a single, generic turn structure, since that treatment ignored lateral diffusion effects as well as field-dependent mobility effects and predicted no dependence on R_c.

Lateral diffusion can be ignored in straight-channel separations due to the fact that the band is essentially homogeneous across the width of the capillary. When the band is tilted, however, it is necessary to consider this effect. Lateral diffusion of tilted bands in the turn will result in a reduction of resolution. The contribution of this lateral diffusion to the band broadening is proportional to the distance required to traverse a turn. The radius of curvature, which is directly proportional to the distance required to traverse a turn, should be as small as feasible to minimize the time spent in the turn.

The electric field dependence of the mobility can become very important in tapered turns because the local field in the constricted region increases by a factor of *n*. At high fields, the dependence of DNA mobility on fragment length becomes marginalized, thus decreasing the efficiency of the column. Using turns with the smallest radius of curvature minimizes this effect.

Taper Geometry. A weaker correlation between the taper length and resolving power was observed (Figure 4D). The data suggest that long taper lengths decrease the resolving power per unit length of the column. Decreasing the length of the taper from 800 to 200 μm produced an increase in the resolution as a function of column length from 0.164 to 0.185 cm^{-1}. Further reduction of l to 55 μm resulted in an increase in resolution to 0.196 cm^{-1}. These results suggest that a tapering element should occupy as little volume in the column as is necessary to link the separation channel to the turn portion.

The effects of capillary tapering have been considered by a number of groups. Holzwarth studied the effects of reducing capillary width on separation efficiency,[23] and Xue and Yeung used a "bubble cell" in which the inner diameter of the capillary is increased to gain longer detection path lengths for absorbance detection.[24] Slais presented a series of papers on CE separations in tapered capillaries.[25−27] Slais[27] concluded that there is a variance

(23) Holzwarth, G. *Electrophoresis* **1996**, *17*, 1587−1589.
(24) Xue, Y. J.; Yeung, E. S. *Anal. Chem.* **1994**, *66*, 3575−3580.
(25) Slais, K. *J. Chromatogr., A* **1994**, *684*, 149−161.
(26) Slais, K. *Electrophoresis* **1995**, *16*, 2060−2068.

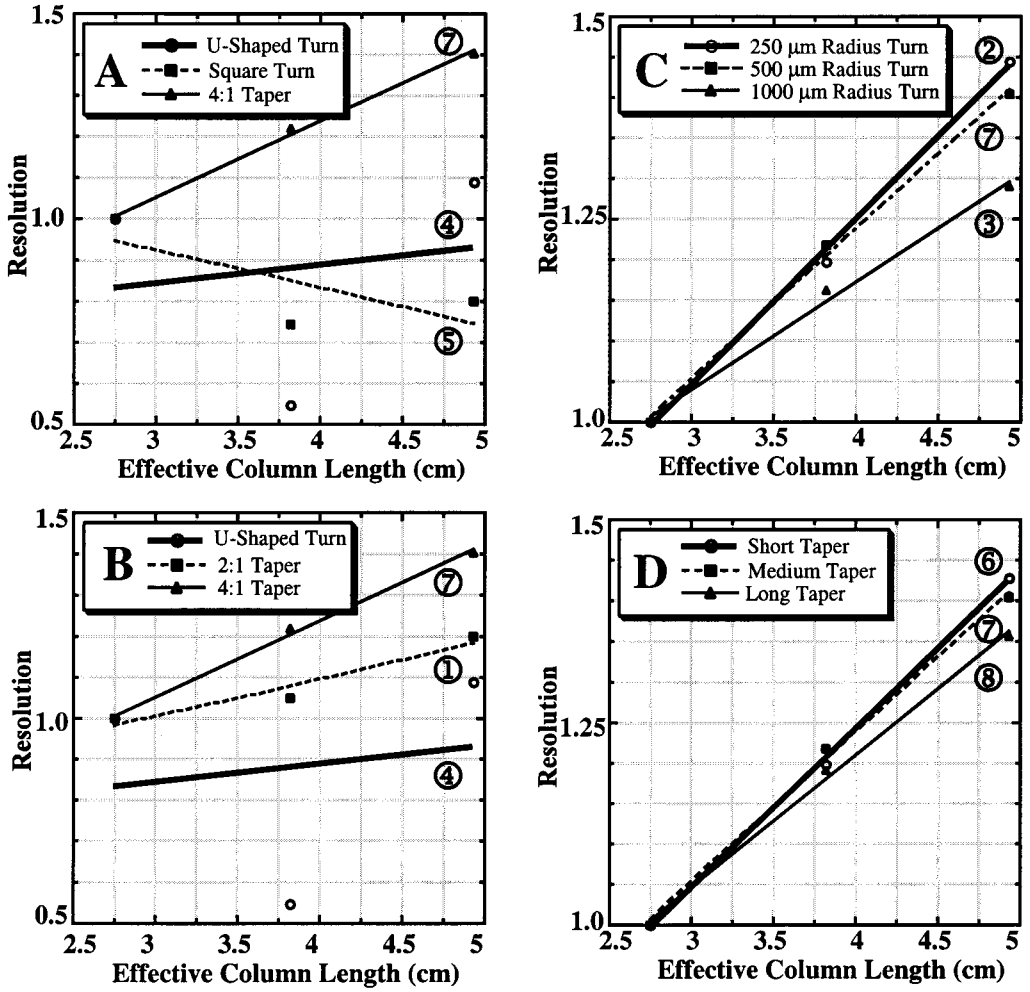

Figure 4. Resolution as a function of effective separation column length for four different experimental comparisons. (A) The effect of turn geometry with R_c fixed at 500 μm. (B) The effect of varying the taper ratio, n, while fixing l at 200 μm and R_c at 500 μm. (C) The effect of varying the radius of curvature, R_c, while fixing l at 200 μm and n at 4. (D) The effect of varying the taper length, l, while fixing R_c at 500 μm and n at 4. The resolution at point x was normalized to 1 for each column design.

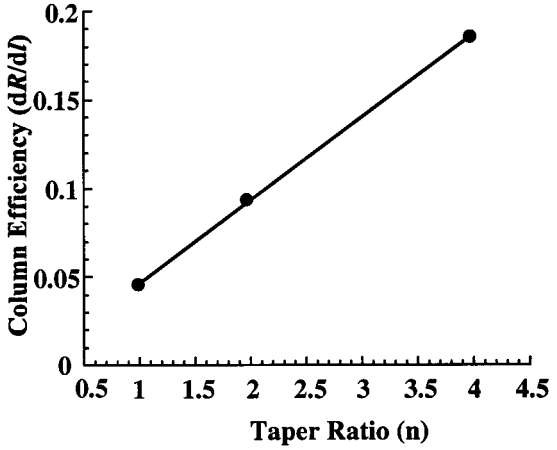

Figure 5. Plot of column efficiency as a function of taper ratio for the separation comparison in Figure 4B ($R^2 = 0.9992$).

associated with tapering the capillary and derived an expression for the effects of local changes in capillary geometry on a Gaussian analyte zone from the continuity equation. The variance, normalized against the variance prior to entering the nonuniform width region described by a funnel-shaped taper, is given by

$$\frac{\sigma^2(t)}{\sigma_0^2} = q^{2t/t_L} + \frac{2Dt_L}{\sigma_0^2}\left(\frac{q^{2t/t_L} - 1}{2 \ln q}\right) \qquad (13)$$

where q is the ratio of the inlet to outlet cross-sectional area (which is equivalent to our n), t_L is the time required for the band to traverse the tapered region, D is the diffusion coefficient of the analyte, σ_0^2 is the band variance prior to entering the taper, and σ^2 is the variance after traversing the taper. The first term in eq 13 describes the length-based variance associated with the conservation of plug volume. This term is irrelevant for our experiment because band expansion at the inlet taper is immediately removed by band compression at the outlet taper. The second term in eq 13 describes the dynamic dispersion of a band as it traverses the region of nonuniform capillary cross section. The dynamic broadening effect is not removed by the outlet taper. It is key to note that t_L is directly related to the taper length for a constant taper ratio. The second term is reduced with shorter l. Further, eq 13 explains the modest sensitivity of our analyses to taper length; the dynamic broadening term is proportional to

(27) Slais, K. *J. Chromatogr., A* **1996**, *730*, 247−259.

t_L/σ_0^2, which has an intrinsically small value in our experiments. For the separations presented, t_L is 0.039 s for the 55-μm taper and 0.57 s for the 800-μm taper, q is fixed at 4, D is 1.0×10^{-5} mm^2/s, and σ_0^2 is 0.0196 mm^2. These values predict that the dynamic broadening variance for the short inlet taper is ~14 times smaller than that for the longest taper consistent with our experimental trends. However, when compared with the initial variance, this term only accounts for 0.3% of the total band variance. Since the experiment indicates that the taper length is more important, we conclude that this theory has not completely captured the effect of the taper on band variance. Factors that are not modeled include the trapezoidal cross section of the channel, surface roughness effects, and field-dependent mobility effects. The most likely explanation for the modest sensitivity of the column efficiency to the taper length is the electric field dependence of DNA mobility. The shorter taper minimizes the transit time of the band in the high electric field region thereby maximizing the column efficiency.

Limit of Maximum Performance. The benchmark for the performance of any column with turns is a straight channel of equal length. Our experiments provide a control point that monitors column performance before any turns have occurred (point *x*). These data may be extrapolated to give the theoretical maximum separation performance of a 4.93-cm straight channel (corresponding to point *z*) using the experimentally determined diffusion coefficient and the electrophoretic mobility of the 271-bp fragment. Assuming that diffusive broadening is the only factor influencing a band traveling in a column with no turns, the band variance, σ_z, may be calculated as

$$\sigma_z^2 = \sigma_x^2 + 2Dt \tag{14}$$

where σ_x is the band variance at point *x*, D is the diffusion coefficient of the 271-bp fragment in 0.75% HEC, and t is the additional time required for the band to travel from point *x* to point *z*. Using eq 14, the number of theoretical plates for a straight channel 4.93 cm in length was computed to be 91 800. The number of theoretical plates observed at point *z* of channel 6 (the highest performance design of those presented) was 83 500. The efficiency compared to the extrapolated straight channel data is 91%. The efficiency of channel 6 using $R_c = 250$ μm is expected to improve slightly to 94%. By combining the most advantageous design parameters in turns, we conclude that channel-folding may be utilized to increase the effective length of a column without significantly compromising the separation performance of the device.

Other Applications. The optimal turn design will, of course, depend on the application. For fragment sizing, we have shown that the width of the channel in the turn is the most critical parameter while R_c and especially l are not as important. In gel-based DNA sequencing applications, the diffusion coefficient of DNA is typically 1−2 orders of magnitude lower,[28] so the diffusive broadening in the turn will be even less important. However, because the mobilities of sequencing fragments become nearly equal at high fields (1200 V/cm) due to biased reptation, a turn with minimal R_c and l should be used for DNA sequencing. The most critical factor in sequencing is decreasing the width of the channel in the turn. In applications involving smaller analytes in less viscous media, the diffusion coefficients may be 2−3 orders of magnitude higher than those in fragment sizing. It has been shown that introducing turns has no observable effect on the separation quality in these CZE applications. This is due to the dominance of diffusional broadening in the expression for band variance, which produces large bands on-column. In this case, both longitudinal and transverse diffusions are so large that the band volume far exceeds the turn volume, and the geometry-related effects described here are negligible in comparison.

CONCLUSIONS

The development of microfabricated chemical analysis devices with more complex designs and increased feature densities will necessitate the use of folded channels that do not sacrifice electrophoretic performance. We have shown that separation quality can be maintained in channels with turns having a small radius of curvature, a short taper length, and a high taper ratio. The "pinched turn" designs presented here will allow the use of folded channels while maximizing the column efficiency. These results will be useful in the development of optimized DNA sequencing CAE microplates with enhanced performance, throughput, and device packing.

ACKNOWLEDGMENT

Fabrication of the CE microplates was performed at the U.C. Berkeley Microfabrication Laboratory. This research was supported by the National Institutes of Health under Grant HG01399 and by the Director, Office of Science, Office of Health and Environmental Research of the U.S. Department of Energy under Contract DEF91ER61125.

Received for review January 13, 2000. Accepted April 25, 2000.

AC000054R

(28) Luckey, J. A.; Norris, T. B.; Smith, L. M. *J. Phys. Chem.* **1993**, *97*, 3067−3075.